galaxies

MDPI

Article

Effects of the Intraday Variability of the Radio Galaxy Perseus A (3C 84) at a Frequency of 6.5 GHz and Evidence for a Possible FRB Event

Vladislavs Bezrukovs [1,*], Oleg Ulyanov [2], Artem Sukharev [1,2], Vyacheslav Zakharenko [2], Mikhail Ryabov [2], Viktor Ozhinskyi [3], Volodymyr Vlasenko [3], Anatolyi Poikhalo [3], Oleksandr Konovalenko [2], Eugene Alekseev [2,4], Mykhailo Palamar [5], Viktor Voityuk [3], Vladyslav Chmil [6], Dmytro Bakun [3], Daniil Zabora [2], Ivar Shmeld [1] and Marina Konuhova [1,7,*]

1 Engineering Research Institute "Ventspils International Radio Astronomy Centre (VIRAC)", Ventspils University of Applied Sciences, Inzenieru 101, LV-3601 Ventspils, Latvia; magister_phys@yahoo.com (A.S.); ivarss@venta.lv (I.S.)
2 Institute of Radio Astronomy, National Academy of Sciences of Ukraine (IRA NASU), Mystetstv 4, 61002 Kharkiv, Ukraine; oulyanov@rian.kharkov.ua (O.U.); zakhar@rian.kharkov.ua (V.Z.); ryabov-uran@ukr.net (M.R.); akonovalenko194@gmail.com (O.K.); ealekseev@rian.kharkov.ua (E.A.); daniil.zabora@stud.onu.edu.ua (D.Z.)
3 National Space Facilities Control and Test Center, State Space Agency of Ukraine, Moskovska 8, 01010 Kyiv, Ukraine; ozvic@ukr.net (V.O.); vlasenko.vp@gmail.com (V.V.); a.poikhalo61@gmail.com (A.P.); w_voytyuk@ukr.net (V.V.); dmytro.bakun@gmail.com (D.B.)
4 UMR 8523–PhLAM (Physique des Lasers Atomes et Molécules), CNRS, University of Lille, F-59000 Lille, France
5 Department of Instruments and Control and Measuring Systems, Ternopil Ivan Puluj National Technical University, 56 Ruska St., 46001 Ternopil, Ukraine; palamar.mi@gmail.com
6 Private Joint Stock Company "Scientific and Production Enterprise "Saturn"", 2B, Les Kurbas Ave., 03148 Kyiv, Ukraine; chmil_vladislav@ukr.net
7 Institute of Solid State Physics, University of Latvia, 8 Kengaraga, LV-1063 Riga, Latvia
* Correspondence: vladislavsb@venta.lv (V.B.); marina.konuhova@cfi.lu.lv (M.K.)

Abstract

Perseus A (3C 84), a powerful radio source located at the centre of the giant elliptical galaxy NGC 1275—classified as a Seyfert type II AGN and the dominant member of the X-ray bright Abell 426 cluster–exhibits radio emission variability over a wide range of timescales, from decades to hours. This study investigates intraday variability (IDV) in the 6.5 GHz radio emission of 3C 84 using the RT-32 radio telescope in Zolochiv, Ukraine. A novel low-amplitude azimuthal scanning method enabled quasi-simultaneous measurements of antenna and system temperatures, allowing for separation of intrinsic source variations from propagation effects. During an observation session in August 2021, a burst with a peak intensity of 13.5 Jy above the background was detected, likely corresponding to a Fast Radio Burst (FRB). Additionally, quasi-periodic low-amplitude variations with timescales from 0.3 to 6 h were observed. These fluctuations correlate strongly with local atmospheric changes, such as dew formation on the telescope structure, and, to a lesser extent, with ionospheric acoustic–gravity waves. The findings highlight the importance of accounting for propagation conditions when interpreting short-timescale radio variability in AGNs and suggest the need for multi-station, multi-frequency monitoring campaigns to distinguish between intrinsic and environmental modulation of AGN flux densities.

Keywords: active galactic nuclei (AGN); fast radio bursts (FRBs); intraday variability (IDV); atmospheric effects; ionospheric scintillation; Perseus A (3C 84); flux variability; radio galaxy; radio telescope; quasi-periodic oscillations

Academic Editor: Phil Edwards

Received: 22 June 2025
Revised: 17 December 2025
Accepted: 18 December 2025
Published: 23 December 2025

1. Introduction

Active galactic nuclei (AGNs) are among the most energetic phenomena in the Universe and have been studied intensively for over five decades. It is now well established that AGNs are powered by the accretion of matter onto supermassive black holes (SMBHs), with masses ranging from millions to billions of solar masses, located at the centres of galactic nuclei—sometimes as single objects, and in some cases, as binary systems. This accretion process, often accompanied by the formation of relativistic jets and energetic outflows, gives rise to intense broadband emission across the electromagnetic spectrum. Over decades of observational and theoretical work, a unified model of AGNs has been developed to interpret their diversity in terms of intrinsic structure, viewing angle, and accretion rate [1,2]. According to this model, AGNs can be classified into several major types, including radio-loud and radio-quiet quasars, Seyfert galaxies (Type 1 and Type 2), and blazars. The classification of Seyfert galaxies is based primarily on the width and intensity of emission lines in their optical spectra. Type 1 (Sy1) Seyferts exhibit broad permitted lines and strong ultraviolet/X-ray emission, while Type 2 (Sy2) Seyferts display narrow permitted and forbidden lines, typically associated with significant nuclear obscuration and enhanced infrared emission [3].

The galaxy NGC 1275, classified as a Sy2 Seyfert galaxy, is one of the most prominent nearby AGNs and the dominant galaxy of the Perseus cluster (Abell 426), one of the brightest X-ray clusters in the sky. It is commonly identified with the compact radio source 3C 84, also known as Perseus A, with a spectral flux density of ~12 Jy at 6 GHz and ~30 Jy at 8 GHz. Its proximity, high radio brightness, and dynamic nuclear activity make it a key target for multi-wavelength AGN variability studies.

Long-term monitoring of 3C 84 has revealed complex variability across multiple timescales, including jet precession and changes in flux density over years to decades [4]. In addition, many AGNs show shorter-timescale variability, including quasi-periodic oscillations on timescales ranging from days to minutes [5,6]. While not strictly periodic, such variability is often characterized by enhanced power at certain timescales in Fourier or wavelet space. Pulsed events of extragalactic origin, now known as Fast Radio Bursts (FRBs), have also been detected in the direction of AGNs (some examples are given in the papers [7,8]); however, there are still very few such works. One of the most important detailed articles on this topic [9] points to the extragalactic location of the FRB source, since a low-luminosity galaxy has been precisely identified in the direction of the burst. These are extremely brief and intense radio pulses, typically lasting a few milliseconds or less, and are often comparable in intensity to or exceeding the steady emission of the host AGN [10,11]. Although similar in form to giant pulsar pulses [12–15], FRBs involve significantly greater energy release [16,17].

The mechanisms responsible for intraday variability (IDV) in AGN radio emission remain under debate. Long-period variations are usually attributed to accretion dynamics, jet orientation, or torus obscuration effects [18,19]. By contrast, IDV can be influenced by propagation effects such as interstellar scintillation, ionospheric disturbances, or rapid structural changes in the radio source itself. Propagation through the Earth's atmosphere introduces additional complications. For example, acoustic–gravity waves (AGWs) in the neutral atmosphere can generate travelling ionospheric disturbances (TIDs), which in turn modulate radio wave propagation [20–23].

One of the most well-developed ideas, both theoretically and supported by a large number of practical observations, is that the IDV at centimetre wavelengths is caused predominantly by interstellar scintillation (ISS) of AGN emission. In the work [24] based on the large-scale MASIV (Micro-Arcsecond Scintillation-Induced Variability Survey) survey, it was found that 56% of all radio sources with flat spectra exhibit rapid variability

(demonstrated variations from 2% to 10% on time scales longer than 2 days). This proves that the phenomenon is very widespread. The data show that the scattering plasma clouds are often located quite close to the Sun (from tens to hundreds of parsecs). This is often associated with the Local Bubble of the interstellar medium. The scattering is not always spherical; plasma structures are often elongated. Traditionally, ionospheric effects were thought to be negligible at frequencies above 1–2 GHz. However, modern high-precision observations, including those using very-long-baseline interferometers (VLBI), indicate that the TEC (Total Electron Content) gradients created by powerful atmospheric waves can introduce phase delays and amplitude distortions even at frequencies up to 10 GHz, especially when observing at low antenna elevation angles, where the effective ionospheric thickness is greatest. Some examples of the ionospheric influence on the propagation of C-band radio waves (~4–8 GHz) are discussed in [25–28]. This does not exclude that even at frequencies of 5–6 GHz, ionospheric effects can have a significant impact on the variability of received AGN emission, taking into account the propagation of AGW during magnetic storms or other active atmospheric processes.

To improve the understanding of short-periodic variations in the spectral flux density of 3C 84, the authors proposed and implemented a joint Latvian–Ukrainian research initiative titled "Joint Latvian–Ukrainian Study of the Peculiar Radio Galaxy Perseus A in Radio and Optical Bands" (PERSEUS)[1]. Within the framework of this project, several observational campaigns were conducted using radio telescopes in Latvia and Ukraine, supplemented by optical observations from telescopes located in Latvia, Ukraine, and Slovakia [29]. This article focuses primarily on the results of the August 2021 observational session carried out with the RT-32 radio telescope in Zolochiv, Ukraine—data which have not been previously reported. During this session, a novel observation technique enabled the detection of IDV in the radio emission of the AGN, with characteristic lifetimes of less than three hours. The results suggest that these short-term fluctuations may primarily be attributed to variations in local weather conditions, including humidity, air temperature, and dew point, and to a lesser extent, to ionospheric AGW and travelling ionospheric disturbances (TIDs).

AGWs can be triggered by various geophysical phenomena, such as earthquakes, volcanic eruptions, nuclear explosions, tsunamis, and the passage of the solar terminator across the Earth's surface. These waves are excited in the lower atmosphere at Brunt–Väisälä frequencies [30,31] and can lead to the formation of TIDs—density wave-like fluctuations in the electron concentration of the ionosphere. The presence of AGWs results in increased kinetic temperatures of "free" electrons and induces oscillations at the same frequencies, manifesting as modulations in both the electron density and velocity.

This process produces three observable effects relevant to radio observations:

1. The spectral flux density of the radio source becomes modulated at the Brunt–Väisälä frequency.
2. The system noise temperature of the radio telescope is also modulated at the same frequency, though with a smaller amplitude.
3. These two modulations occur approximately in anti-phase. This is because the ionospheric plasma along the line-of-sight acts as a time-varying semi-transparent refractive screen (i.e., with variable dielectric constant). When this "plasma mirror" is more transparent, the recorded signal from the astronomical source increases, while the contribution of scattered terrestrial radio emission decreases. Conversely, when the transparency is reduced, the observed flux from the source decreases, and the contribution from Earth's own emission increases.

As a result, the observer should register a classical scintillation pattern produced by multipath interference from ionospheric irregularities. Although the average flux

density remains almost unchanged, interference minima and maxima in the radio emission intensity—caused by multipath propagation—appear in the response of the radio telescope. The effect of AGW on the spectral flux density of the radio source may be small. But the third consequence described above makes it possible to detect these waves as a negative correlation between antenna temperature fluctuations and the temperature of the radio telescope's self-noise at zero lag.

Additional environmental effects, such as dew formation on the radio-transparent coating of the antenna or its beam waveguide tube (in Beam Wave Guide (BWG) telescope systems), can also attenuate the source brightness temperature without significantly affecting the telescope's internal system noise. In contrast, water clouds or precipitation increase system noise and reduce the apparent brightness temperature of the source.

This article presents and analyses observational data collected with the RT-32 radio telescope in Zolochiv (Lviv region, Ukraine) during the period 22–27 August 2021, along with selected data from other sessions. On the night of 22–23 August 2021, at approximately 04:37:05 UTC, a transient burst was recorded with internal fine structure, consistent with an FRB. The article applies spectral, cross-correlation, and wavelet analysis to interpret the variability signatures observed in 3C 84. The results support the hypothesis that low-intensity, short-periodic variations in AGN radio flux may be significantly influenced by meteorological factors—particularly dew formation on the beam guide structure of the RT-32 telescope. An upper limit is also estimated for the contribution of AGW/TID phenomena to short-term flux density fluctuations at mid-latitudes in the absence of major seismic or volcanic activity.

2. Observation Technique for Quasi-Simultaneous Measurement of Antenna and System Temperatures

2.1. Description of the Radio Telescope RT-32 Zolochiv

To observe the source 3C 84, we used the RT-32 radio telescope located in Zolochiv, Ukraine. This instrument was originally constructed as a MARK-B telecommunications antenna by the Japanese corporation NEC [32]. Antennas of similar design have been adapted for radio astronomy in New Zealand and Japan. The process of converting such telecommunication antennas into functioning radio telescopes is described in detail in [33–38].

Galactic maser sources were used to calibrate the radio telescope. The calibration procedure, based on observations of these sources, is described in detail in [36–38], including a complete account of all stages of the RT-32 Zolochiv upgrade for radio astronomical observations and calibration tests.

The RT-32 is a Beam Wave Guide (BWG) type antenna equipped with a corrugated horn, similar in design to antennas employed by NASA's Deep Space Network [39,40]. BWG antennas offer several advantages:

1. All receiving and recording equipment can be placed in a stable environment on the ground, mounted on a separate monolithic foundation.
2. The corrugated horn supports wide operational bandwidths across several bands (C (4.7–6.8 GHz), X (9.5–12 GHz) and K (20–25 GHz) in our case).
3. The beam pattern maxima are co-aligned across these frequency bands, unlike in offset-fed antennas.
4. The secondary focus lies below the beam guide aperture, partially shielding the receiver from thermal radiation originating from the ground.

However, BWG antennas also have certain disadvantages:

1. The presence of at least four additional reflecting surfaces in the beam guide path increases the total surface roughness, which reduces the maximum usable frequency compared to two-mirror systems.
2. The effective system temperature includes a contribution from the beam guide's thermal background.
3. The relatively small diameter of the beam guide (typically <2.5 m) imposes diffraction limitations at lower frequencies (f < 2.3 GHz).

The main parameters of the RT-32 radio telescope are shown in Table 1.

Table 1. The main parameters of the radio telescope RT-32 Zolochiv: the telescope name (RT name), observing centre frequency (F_{obs}), bandwidth (ΔF), beamwidth (λD), rms pointing error ($\sigma(\lambda D)$), scan period (ΔT_{sc}), scan length (T_{sc}), scanning amplitude in azimuth (SAA), date of observation (Date).

Date	SAA, deg	ΔT_{sc}, s	Tsc, m	$\sigma(\lambda/D)$, ''	λ/D, '	ΔF, GHz	F_{obs}, GHz	RT Name
22–27 August 2021	0.5	120	30	36	6	0.5	6.5	RT-32 (Zolochiv)

2.2. Observations Using the Azimuthal Scanning Mode

The RT-32 radio telescope supports multiple scanning modes, including elevation scanning, ephemeris tracking, and azimuth scanning, all of which can be employed for continuous source tracking. The antenna has an azimuthal rotation range of $\pm 270^\circ$ and an elevation angle range from 5° to 90°. Elevation and ephemeris scanning modulate the antenna temperature, as thermal noise from the Earth increases at lower elevation angles. In contrast, rapid azimuthal scanning with a small amplitude (up to 0.5°) introduces negligible change in elevation angle and therefore contributes minimally to system noise. This feature enabled us to implement a quasi-simultaneous measurement scheme for 3C 84, using azimuthal scans every 30 min with a scanning amplitude of 0.5° and a period of 120 s. Previously measured azimuth and elevation pointing error matrices were uploaded into the RT-32 control system [41].

The RT-32 radio telescope in Zolochiv is particularly well-suited for studying IDV, owing to its high sensitivity, low system noise, and low levels of external radio interference. Its design allows for simultaneous dual-frequency, dual-polarization observations with time resolutions of one or ten measurements per second. These capabilities, along with the antenna's favourable geographic location, make RT-32 effective instrument for IDV research. At 6.5 GHz, the RT-32 has a beamwidth of approximately 6 arcminutes. The root mean square (RMS) pointing error is approximately 36 arcseconds. With a surface efficiency of $\eta \approx 0.7$, the effective collecting area of the telescope is $A_{eff} \approx \pi R^2 \eta \approx 560$ m^2.

Figures 1–3 show the results of azimuthal scans of 3C 84 conducted between 22 and 27 August 2021. The central observing frequency was 6.5 GHz with a bandwidth of 0.5 GHz. Fourth-degree polynomial envelopes were fitted to the maximum and minimum responses of each scan using a minimum standard deviation method.

This observation technique enables the quasi-simultaneous estimation of both the antenna temperature (upper envelope) and the system noise temperature (lower envelope) during each azimuthal scan interval (~120 s). Although the measurements are not truly simultaneous—being separated by the scan period—they are sufficiently close in time to allow meaningful comparisons. Between scans, both temperature dependencies can be interpolated using the nodal points of the envelopes to reconstruct their temporal evolution. This approach provides a continuous time series of the brightness temperature of the radio source and the background system temperature.

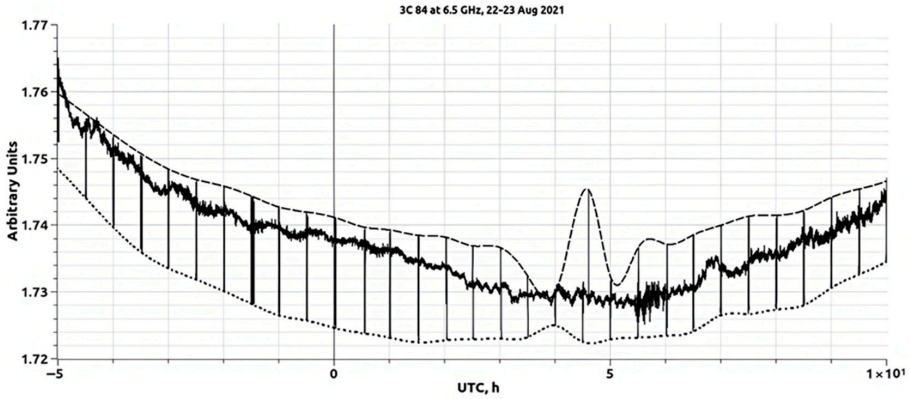

Figure 1. Response of the RT-32 radio telescope (in arbitrary units) during azimuthal scanning of the radio source 3C 84, conducted every 30 min on the night of 22–23 August 2021. The upper envelope (dashed line) is drawn through the local maxima of each scan, including a prominent peak near 04:37:05 UTC, while the lower envelope (dotted line) follows the local minima corresponding to each azimuthal pass. Both envelopes are modelled using fourth-order polynomials fitted by the method of minimum standard deviation.

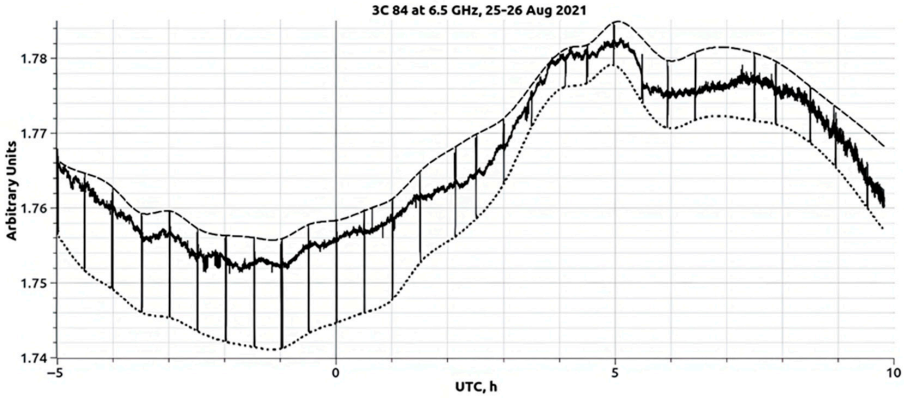

Figure 2. Response of the RT-32 radio telescope (in arbitrary units) during azimuthal scanning of the radio source 3C 84, conducted every 30 min on the night of 25–26 August 2021. The upper envelope (dashed line) traces the local maxima of the scans, and the lower envelope (dotted line) follows the corresponding minima. Both envelopes are fitted with fourth-order polynomials using the minimum standard deviation method.

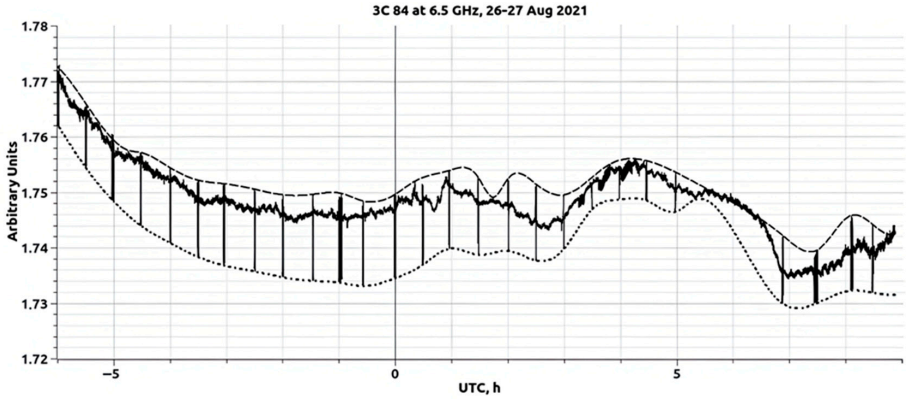

Figure 3. Response of the RT-32 radio telescope (in arbitrary units) during azimuthal scanning of the radio source 3C 84, conducted every 30 min on the night of 26–27 August 2021. The upper envelope (dashed line) traces the scan maxima, and the lower envelope (dotted line) follows the corresponding minima. Both envelopes are fitted with fourth-order polynomials using the minimum standard deviation method.

An important advantage of this method is its ability to suppress high-frequency flux fluctuations with quasi-periods shorter than 10 min. Such fluctuations are commonly caused by environmental and instrumental factors, including wind gusts, mechanical backlash in the telescope drive system, or interplanetary scintillation. These sources of noise can obscure the detection of intrinsic variability in AGNs, particularly in the sub-hour domain. Since variations on timescales shorter than 10 min are generally not observed in AGN light curves and are rarely described in the literature, their removal enhances the reliability of the extracted signal. Notably, fluctuations with periods below this threshold may still arise from propagation effects, such as ionospheric scintillations (T > 1 s) and interplanetary scintillations (T ~ 0.1 s), which this method helps to identify and isolate.

This technique offers multiple advantages. Conventionally, only a single curve (the upper envelopes in Figures 1–3) is used to represent the antenna temperature from the direction of the source. In these figures, the horizontal axis shows time in hours from 00:00 UTC, and the vertical axis shows the intensity in arbitrary units. Here, we analyze both the upper and lower envelopes. The lower envelope represents the system noise temperature in the absence of the source, including the sky background. The difference between these envelopes provides a direct estimate of the source's brightness temperature, under the assumption that its angular size is significantly smaller than the beam. According to studies of the angular structure of the radio source 3C 84, its angular size is approximately 125 μas at 5 GHz [42,43]. Given the beamwidth of the RT-32, 3C 84 can be considered a point source. The envelope difference thus reflects the "pure" signal from 3C 84. This approach enables not only spectral and autocorrelation analysis of the flux and system noise temperature but also the construction of cross-correlation functions between them—yielding additional insight into propagation effects and variability.

The root-mean-square (RMS) pointing accuracy of the RT-32 during the observation interval was 36 arcseconds. To improve the accuracy of the spectral flux density estimates, fast scans of the source were performed every 30 min. Consequently, the upper peaks correspond to estimates of the brightness temperature in the source core plus the receiver system noise temperature of the entire RT-32 signal chain. The lower peaks likewise represent estimates of the background temperature plus the receiver system noise temperature. The difference between these curves no longer contains the contribution of the system noise and thus provides a "pure" estimate of the source brightness temperature (as shown above, given the beamwidth of the RT-32, the radio source 3C 84 can be considered a point source).

The appearance of sharp maxima during scans (e.g., in Figures 1–3) indicates that the RT-32 beam maximum is systematically offset from the ephemeris position in azimuth. The upper envelope (dashed line) corresponds to the antenna temperature during accurate pointing at 3C 84, while the lower envelope reflects the system noise when the source is outside the beam. The angular offset between these responses is less than 0.5°. The time-dependent difference between the envelopes characterizes the brightness temperature variations of 3C 84. A strong intensity peak observed on 23 August 2021 at approximately 04:37:05 UTC is analyzed in detail in a subsequent section.

2.3. Observations of Intraday Variability in Radio Source Tracking Mode

For the observations of intraday variability (IDV) of the radio source 3C 84, the classical source-tracking method was employed. The measurements were carried out with a broadband radiometer in two circular polarizations (left-hand, LCP, and right-hand, RCP). The initial temporal resolution was 0.1 s; however, since this was somewhat redundant, the data were decimated to a 1 s time step. This choice is convenient because it allows the digital frequency in the spectral analysis of the time series to be expressed directly in hertz.

The longest IDV monitoring sessions were conducted in August 2021. At the latitude of Zolochiv, the maximum elevation of 3C 84 above the horizon was ~81°, while the minimum was ~22°, making this radio source particularly suitable for long-duration tracking observations of up to ~15 h continuously.

The observations were performed at frequencies of 5 and 6 GHz. The radiometer output provided signal amplitudes in volts (V), which were subsequently converted into decibels (dB). Knowing the parameters of the radio telescope, the flux density can be derived in terms of antenna temperature (K) and then converted into Janskys (Jy). The estimated mean flux density in August 2021 was approximately 27 Jy.

The raw signal curve of 3C 84 exhibits a smooth arc-like shape. At low antenna elevations, the total flux received increases due to the contribution of near-surface radio noise entering through the sidelobes of the antenna beam pattern. At higher elevations, the flux decreases, as the contribution of noise through the sidelobes diminishes. An example of the raw signal record is shown in Figure 4.

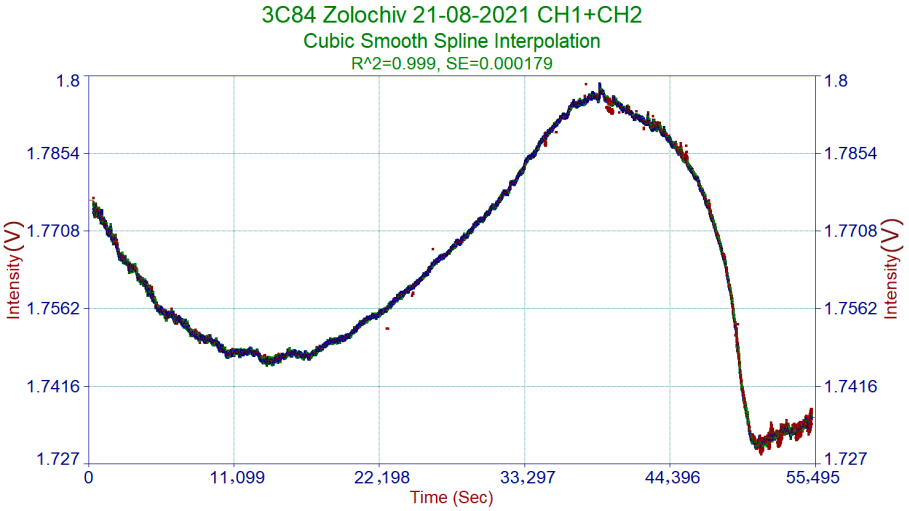

Figure 4. The original raw intensity light curves of the source 3C 84 (averaged over the two polarization channels—green and brown dots), approximated using a smooth cubic spline (dark blue line) obtained on 21 August 2021 at 5 GHz. Small-scale fluctuations superimposed on the trend-like curve represent fast variability. In this example, R^2 = 0.999 and SE = 0.000179 indicate high accuracy of the cubic spline approximation. Green dots indicate points within 3σ chi-square (close to the trend), while brown dots show high deviations from the trend.

Before digital spectral analysis, a standard time series transformation was performed—subtracting the mean and dividing by the standard deviation. This is an important procedure to ensure that the time-frequency spectra do not contain a strong constant component and that the colour palette of intensities is approximately uniform. To remove the elevation-dependent trend, it is common practice to subtract a low-order polynomial that describes the trend. In our case, however, a Savitzky–Golay polynomial filter [44] was applied to the spline-interpolated data, providing a more accurate extraction of the high-frequency component of the signal time series. Figure 5 shows an example of the curve of rapid intensity variations of the radio source 3C 84 after their extraction using the Savitzky–Golay filter.

These curves of rapid radio signal variations became the basis for the study of intraday variability in Section 3.2, and the results with examples of digital spectral analysis are given further in Section 3.2.

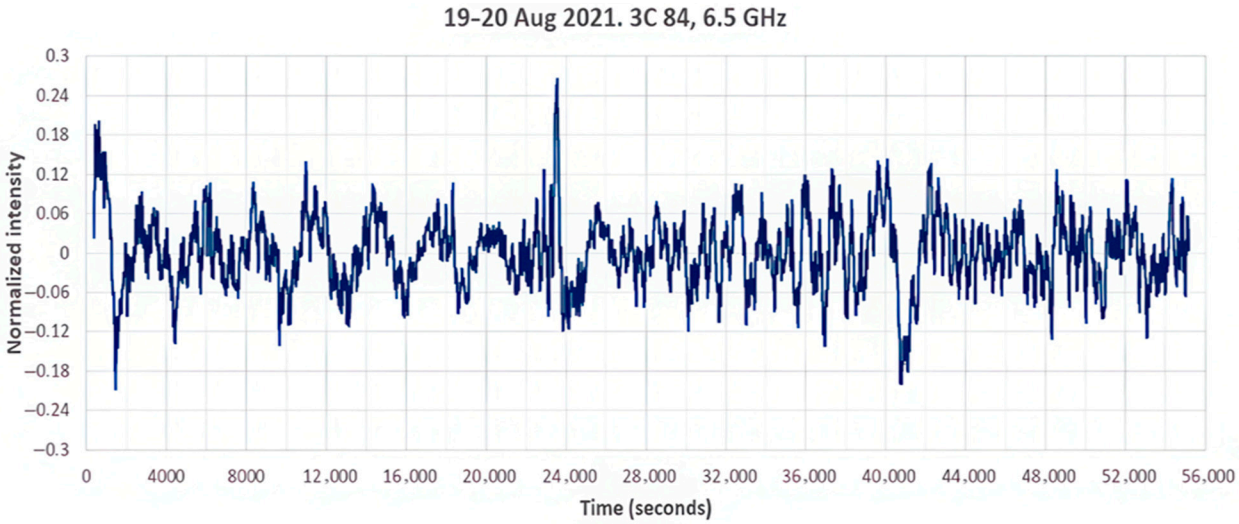

Figure 5. Rapid variations in the radio emission from 3C 84 at 6.5 GHz, extracted using the Sa-vitzky–Golay filter, during the observing session of 19–20 August 2021, with a duration of ~15 h.

3. Results and Interpretation of Observational Data

3.1. Evidence for an FRB from the Direction of 3C 84

In radio astronomy, an FRB is defined as a transient, high-intensity radio pulse with a duration ranging from a fraction of a millisecond (in the case of ultrafast FRBs) up to several seconds [45], typically attributed to high-energy astrophysical processes. The physical origin of FRBs remains uncertain, and various hypotheses have been proposed. These include magnetar outbursts, mergers of neutron star binaries, star-forming region activity, and interactions involving active galactic nuclei (AGNs), such as high-energy relativistic jets impacting nearby gas clouds in galactic centres [46]. However, these interpretations remain under debate and require further investigation based on a larger dataset of well-characterized FRB events.

From our perspective, the most intriguing results were obtained during the observation session of 22–23 August 2021. At 04:37:05 UTC, a transient burst was detected from the direction of 3C 84. The active phase of this event lasted approximately 3 s, displaying internal substructure with intensity variations on timescales of 0.2–0.3 s (see Figure 6). As this signal was recorded using a broadband detector, no spectral resolution was available for detailed frequency-domain analysis.

Three possible explanations were considered for the origin of this burst. First, it could be attributed to internal or external radio frequency interference. However, throughout more than a year of systematic observations of 3C 84 using the same system, we did not observe similar internal interference signatures. External interference, such as telemetry signals from artificial satellites, is a theoretical possibility, especially if the satellite signal entered through a side lobe of the antenna beam. If the signal had entered through the main lobe, its amplitude would likely have been several orders of magnitude higher. Furthermore, no comparable external interferences were observed at elevation angles exceeding 20°, whereas the elevation angle during the burst exceeded 60°. Satellite telemetry signals are typically of low intensity and unlikely to produce the observed burst characteristics.

The second possibility is that the burst represents short-lived radio emission phenomena such as ionospheric scintillation, maser or megamaser flares, or a fast radio burst (FRB). Given the short duration and temporal structure of the signal, scintillation and maser events seem less plausible. Therefore, assuming an extragalactic origin, we suggest that the signal most likely corresponds to a fast radio burst associated with the AGN 3C 84.

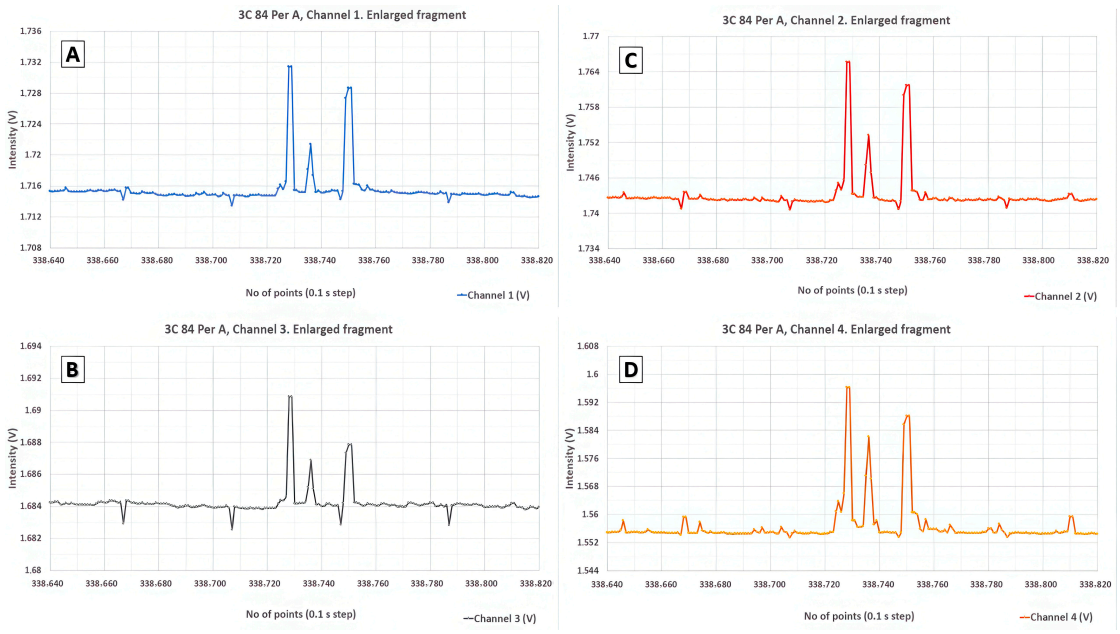

Figure 6. Pulsed radio emission detected from the direction of the radio source 3C 84 on 22–23 August 2021. The left panel shows time series data from the first frequency channel: right circular polarization (**A**) and left circular polarization (**B**). The right panel presents corresponding data from the second frequency channel: right circular polarization (**C**) and left circular polarization (**D**). The temporal resolution is 0.1 s per data point.

We explore this interpretation below. The broadband detector used in our system did not apply any dispersion delay compensation. To estimate the potential effect of dispersion, we assume a characteristic dispersion measure (DM) of 500 pc·cm^{-3}, which is typical for extragalactic FRB sources. The expected dispersion delay $\Delta\tau_{DM}$ between 6.25 GHz and 6.75 GHz is calculated using the standard formula:

$$\Delta\tau_{DM} = \frac{DM}{M} \cdot \left(\frac{1}{f_L^2} - \frac{1}{f_H^2} \right), \tag{1}$$

or in practical units:

$$\frac{\Delta\tau_{DM}}{sec} = \frac{0.415DM}{pccm^{-3}} \cdot \left(\frac{1}{(f_L/100MHz)^2} - \frac{1}{(f_H/100MHz)^2} \right) = 0.00758 \tag{2}$$

where

$\Delta\tau_{DM}$—is the dispersion delay time in seconds for a wideband pulse between 6.25 GHz and 6.75 GHz,

$$M = 2\pi m_e c/e^2, \tag{3}$$

m_e—the electron rest mass,
c—is the speed of light in vacuum,
e—is the electron charge,
DM = 500 pc·cm^{-3}, is the characteristic value of the dispersion measure for extragalactic sources,
f_L and f_H—is the low and high frequencies in Hz.

The estimated dispersion delay, ($\Delta\tau_{DM} \approx 0.0076$ s, is approximately 22.5 times smaller than the detector's time resolution of 0.1 s, meaning that any intra-channel dispersion would not be resolved. The broadband detector recorded signals in both right and left circular polarizations across two frequency channels. The centre frequency of the first

channel was 6480.033 MHz, and that of the second was 6544.852 MHz, corresponding to a channel separation of 64.819 MHz. The pulse structure was clearly visible in all four data streams, with well-correlated temporal profiles and only minor amplitude differences (see Figure 6). Over a ~3 s interval, the recorded flux intensity between local maxima significantly exceeded the background level—consistent with the emission profile of fast radio bursts reported in the literature [47,48].

An alternative explanation for the recorded phenomenon could involve ionospheric scintillation caused by spatial inhomogeneities in the electron density of the Earth's ionosphere. In this interpretation, the observed burst might correspond to a transient structure in the F2 layer, potentially formed during the passage of the solar terminator.

Modern models of the ionosphere assume the presence of ionized layers D, E, F (the last, uppermost layer, under different ionization conditions can be divided into layers F1 and F2). More details about the ionospheric layers are presented in the works [49,50].

The timing of the intense response indeed coincides with the local terminator crossing, making this hypothesis worth consideration. Under this assumption, the upper and lower envelopes of the signal could be interpreted as shown in Figure 7.

However, we consider this scenario unlikely. First, the intensity recorded to the left and right of the pulse (Figures 1–3 and 6) does not exceed the background level, suggesting the absence of a broader enhancement that would typically accompany ionospheric restructuring. Second, the time of the pulse is offset from the scan midpoint by several minutes, indicating that the burst was short-lived and not quasi-periodic. Moreover, the formation and restructuring of the F2 layer at the night–day boundary generally occurs over longer timescales—significantly exceeding the ~3 s duration of the observed event. Therefore, we do not associate this pulse with ionospheric processes and consider an extraterrestrial origin, such as an FRB, to be more plausible. The detected burst exhibited properties consistent with those of an FRB, although further observations with good temporal resolution will be needed for confirmation. To confidently confirm that a recorded event is an FRB, its dynamic spectra should be obtained. If dispersive time delays are detected for the same impulsive components in these spectra (e.g., [51]), the event can be reliably identified as an FRB.

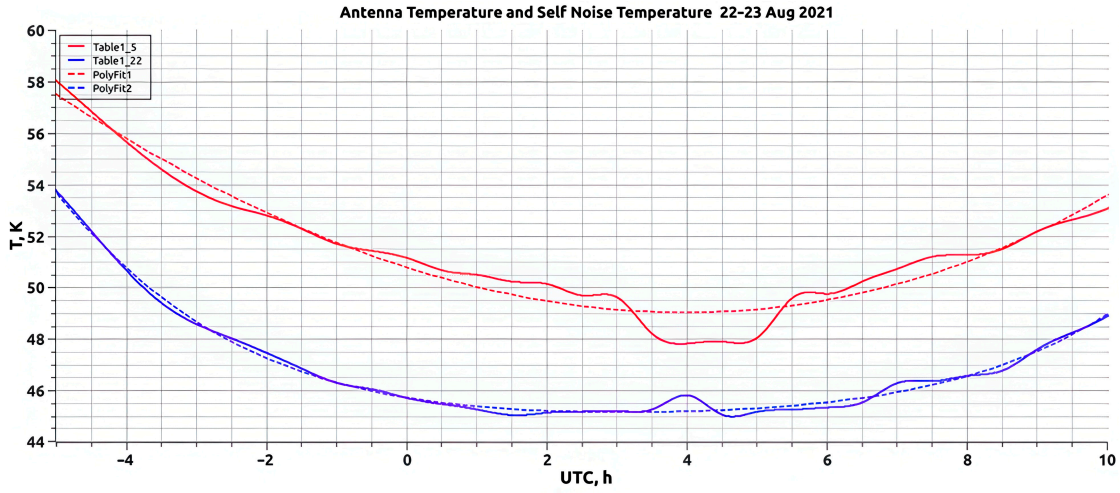

Figure 7. Estimated antenna temperature in the direction of the radio source 3C 84 (solid red curve) and the system self-noise temperature of the RT-32 radio telescope (solid blue curve) based on azimuthal scanning observations from 22 to 23 August 2021. Fourth-degree polynomial fits to each temperature curve are shown as dashed lines in the corresponding colours. The transient burst detected at 04:37:05 UTC on 23 August 2021 has been excluded from the dataset.

3.2. Ionospheric Waves and Weather Effects as Possible Drivers of Intraday Variability in 3C 84

For further analysis, we recalculated the RT-32 (Zolochiv) telescope response from arbitrary units into antenna temperature and subsequently into spectral flux density. In this approach, the spectral flux density of the radio source 3C 84 is considered proportional to the difference between the antenna temperatures represented by the upper and lower envelopes (see Figure 7). For the clearest data obtained on the night of 22–23 August 2021, the minimum antenna temperature corresponds to the system noise temperature (T_{sys}) of the RT-32 receiver and backend system. Based on our earlier calibrations [36–38], we estimate $T_{sys} \approx 45 \pm 0.5$ K at this operating frequency. Using this value and the known effective collecting area of the RT-32 telescope, we converted the temperature difference between the envelopes into the spectral flux density of 3C 84. These results are presented in Figures 8 and 9, where the zero point on the horizontal axis corresponds to the UTC midnight transition.

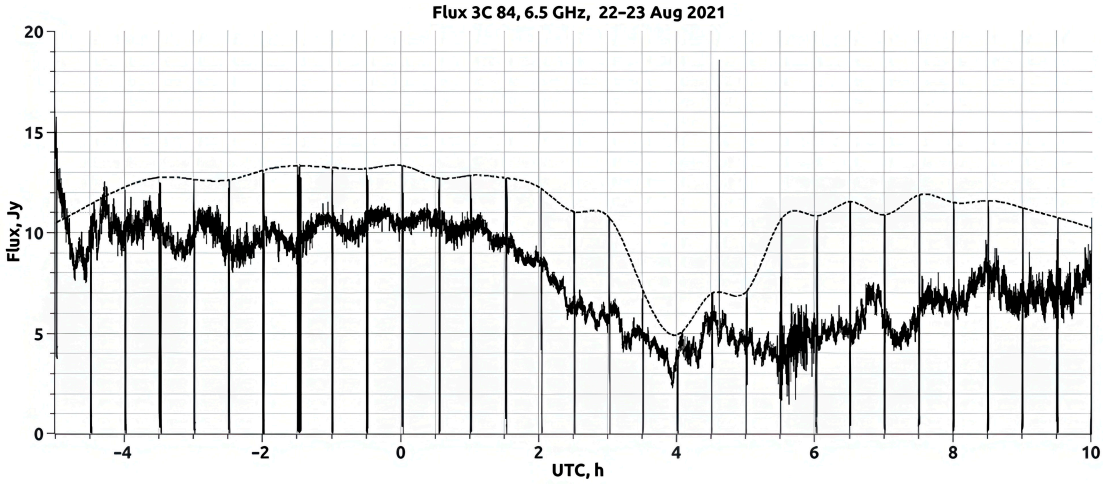

Figure 8. Estimated spectral flux density of the radio source 3C 84 at a frequency of 6.5 GHz, based on observations conducted on 22–23 August 2021. The solid curve represents the measured flux density derived from antenna temperature differences, while the dashed curve corresponds to a smoothed approximation using polynomial fitting.

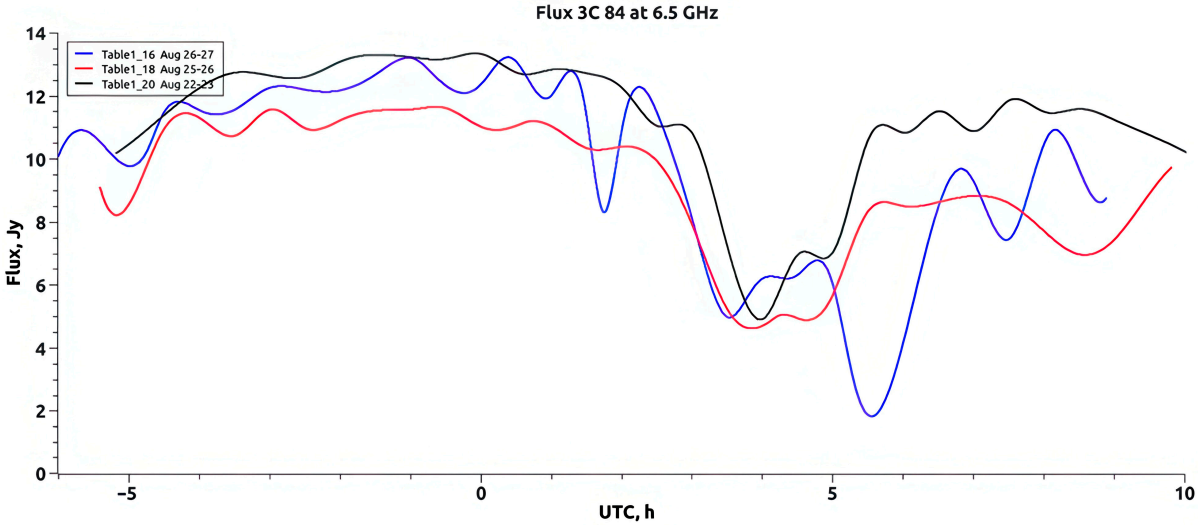

Figure 9. Estimated spectral flux density of the radio source 3C 84 at a frequency of 6.5 GHz from three observational sessions: 22–23 August 2021 (black curve), 25–26 August 2021 (red curve), and 26–27 August 2021 (blue curve). The transient pulse event recorded at 04:37:05 UTC on 23 August 2021 has been excluded from the data.

From Figures 8 and 9, it is evident that starting around 03:00 UTC, a significant drop in spectral flux density is observed. This decrease lasts approximately 2.5 h on both 22–23 and 25–26 August 2021, while on 26–27 August it extends even longer. To interpret these results, we compared the RT-32 measurements with meteorological data from an automatic weather station located approximately 50 m from the telescope, mounted on the roof of a nearby building. We specifically examined ambient air temperature, relative humidity, and dew point. These meteorological variables for 22–23 August 2021 are shown in Figure 10, along with corresponding fluctuations in the brightness temperature of 3C 84 and in the system noise temperature of RT-32.

During the nighttime and early morning hours (Ukrainian summertime: UTC + 3), the difference between the ambient temperature and the dew point was minimal—typically between 0.5 and 1.0 °C. Concurrently, relative humidity peaked at 94–96% and began to decrease only after sunrise. Atmospheric pressure increased gradually from 754.5 mmHg to 759.5 mmHg. Given the sensor offset relative to the radio-transparent feed enclosure of the RT-32 (both horizontally and vertically), we assume that dew condensed on the feed system's dielectric cover as well as on the metallic surface of the primary reflector. It is likely that dew formation began around 02:30 UTC and persisted until approximately 05:30 UTC on both 22–23 and 25–26 August. In our interpretation, the primary factor contributing to the observed reduction in spectral flux density of 3C 84 during this interval is dew accumulation on key components of the antenna structure.

Between 02:00 and 06:00 UTC, the brightness temperature of 3C 84 and the system noise temperature exhibited a temporal offset. We quantified this offset via cross-correlation analysis of the two envelope curves, after removing fitted fourth-order polynomials using the minimum standard deviation method (see Figure 7). The resulting lag was slightly greater than one hour (see Figure 11). The cross-correlation coefficient between the two time series was negative at zero lag, suggesting anticorrelated behaviour under non-stationary ionospheric conditions. Additionally, the local minimum of the correlation function was shifted by slightly less than one hour from zero, implying a quasi-periodic interaction between the ionospheric fluctuations and observed radio flux. The total width of the negative correlation window is about two hours, consistent with the duration of the brightness temperature decrease observed in Figures 7–9.

Assuming that the observed negative correlation coefficient at zero lag ($\rho \approx -0.25$) is due solely to AGW and TID effects, and knowing the standard deviations of brightness temperature fluctuations ($\sigma(T_{3C84}) = 0.527$ K) and system noise temperature ($\sigma(T_{sys}) = 0.175$ K), we can estimate the upper limit of AGW/TID power, expressed in temperature units. we can estimate the upper limit of AGW/TID power, expressed in temperature units:

$$T_{AWG/TID} \sim |\rho| \cdot [\sigma(T_{3C84}) \cdot \sigma(T_{sys})]^{1/2} \leq 0.076 \text{ K} \quad (4)$$

This result indicates a weak but measurable ionospheric effect on the received flux. No significant earthquakes were recorded at the time of observation according to global seismic monitoring[2], and all sources of volcanic activity were geographically distant. Therefore, the observed AGW/TID effects may be linked to solar terminator dynamics rather than seismic or volcanic sources.

To further explore variability patterns, we performed Fast Fourier Transform (FFT) analysis on the 3C 84 brightness temperature time series. The input signal was computed as the difference between the upper and lower envelopes—representing the "pure" astrophysical signal from 3C 84. The FFT spectra are shown in Figure 12. All spectra exhibit enhanced power in a specific frequency band. A well-defined local maximum was detected on 22–23 August 2021 at approximately 1.82×10^{-4} Hz, corresponding to a quasi-period $P \approx 5488$ s ≈ 1.52 h. The full width of the spectral feature spans the frequency interval from

~0.5 × 10^{-4} Hz to 1 × 10^{-3} Hz, or a timescale range of ~0.27 to ~5.56 h. Similar features were observed on other nights, confirming that the quasi-periodic variations are real and not attributable to instrumental noise or external interference.

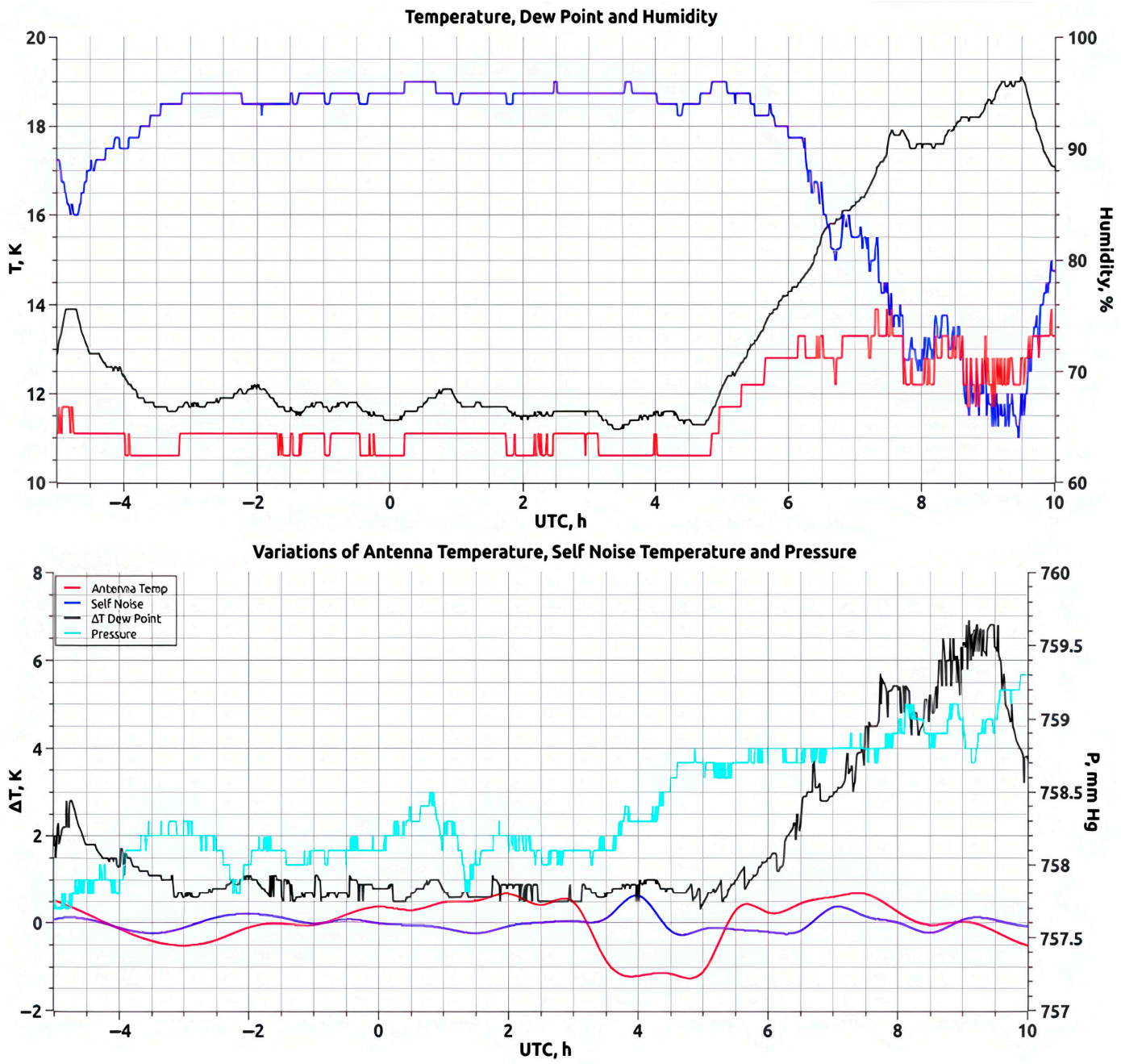

Figure 10. Meteorological and radio observational data from 22 to 23 August 2021. (**Top panel**): Time evolution of ambient temperature (black curve), dew point temperature (red curve), and relative humidity (blue curve). (**Bottom panel**): Difference between ambient temperature and dew point (black curve), fluctuations in the brightness temperature of the radio source 3C 84 (red curve), fluctuations in the self-noise temperature of the RT-32 radio telescope (blue curve), and atmospheric pressure (light blue curve). Temperature fluctuations were calculated as deviations from a fourth-degree polynomial fit to each corresponding temperature curve, as illustrated in Figure 7.

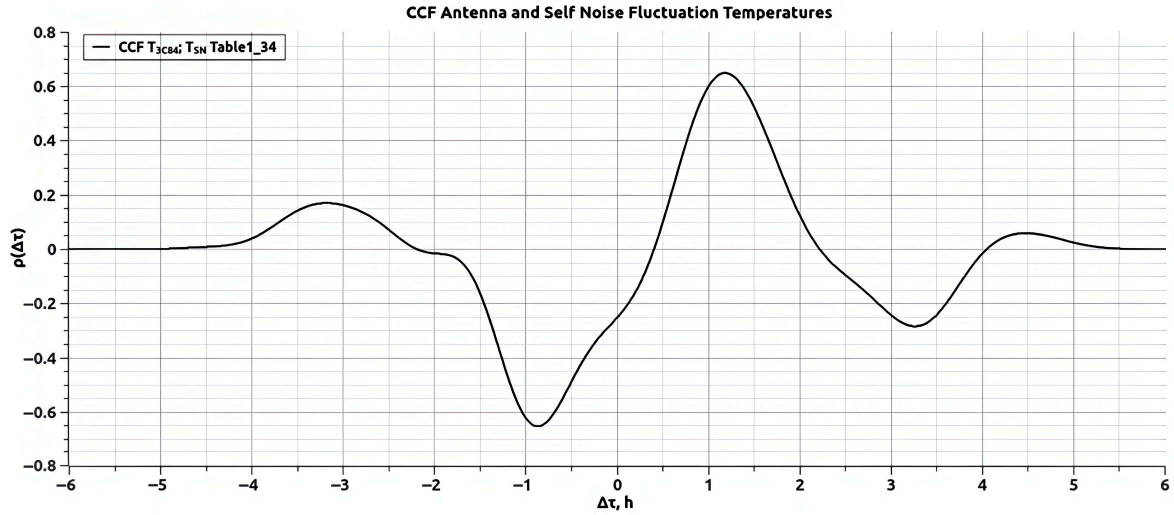

Figure 11. Cross-correlation function between the brightness temperature fluctuations of the radio source 3C 84 and the intrinsic system noise temperature of the RT-32 radio telescope, computed using a sliding time window of approximately 4 h.

Although the intensity of these spectral features is relatively low, their reproducibility suggests an underlying physical origin. At this stage, we cannot definitively identify the dominant mechanism responsible for these quasi-periodic variations. However, future studies using multi-antenna systems operating across widely spaced frequency bands may provide further insight into the nature of intraday variability in AGN radio emission.

As described above, AGW and TID may induce low-intensity, rapid variations in the radio signal from the source 3C 84, within a range of quasi-periods from one to six hours. In this section, we examine wavelet spectral features to gain further insight into the time–frequency structure of the variability. Unlike the previously discussed azimuthal scanning method, the examples here are based on conventional tracking observations.

To generate digital time-frequency spectra, we used a fast continuous wavelet transform (CWT) method with Morlet and Gaussian Derivative wavelets as the analyzing functions. The wavelet transform was computed via convolution of the input time series with scaled and shifted versions of the mother wavelet, using a Fast Fourier Transform (FFT)-based approach [52,53].

To construct the wavelet spectra, the following parameters were used: FFT lengths of 131,072 and 65,536, wave numbers of 12 for the Morlet wavelet and 60 for the Gaussian Derivative wavelet; complex wavelets were employed; the magnitude was calculated as $\sqrt{\Re^2 + \Im^2}$, and the power spectral density (PSD) was calculated as $2\left(\Re^2 + \Im^2\right)$, where $\Re$ and $\Im$ are the real and imaginary components, respectively, of the continuous wavelet transform. To extract period bands from the signal for subsequent spectral construction, a Fourier bandpass filter with a Hamming spectral window was used. This window is optimal for bandpass FFT-filtering; it provides clean filtering and reduces masking of weak signals by strong adjacent frequencies.

During 2021, monthly monitoring showed significant variation in IDV activity. In some months, clear episodes of IDV were observed, while in others, only irregular, noise-like fluctuations occurred. In August 2021, variations on timescales of ~1 h were more prevalent than those on longer timescales of 3–7 h. An example of wavelet spectra illustrating variability in 3C 84 is presented in Figure 13.

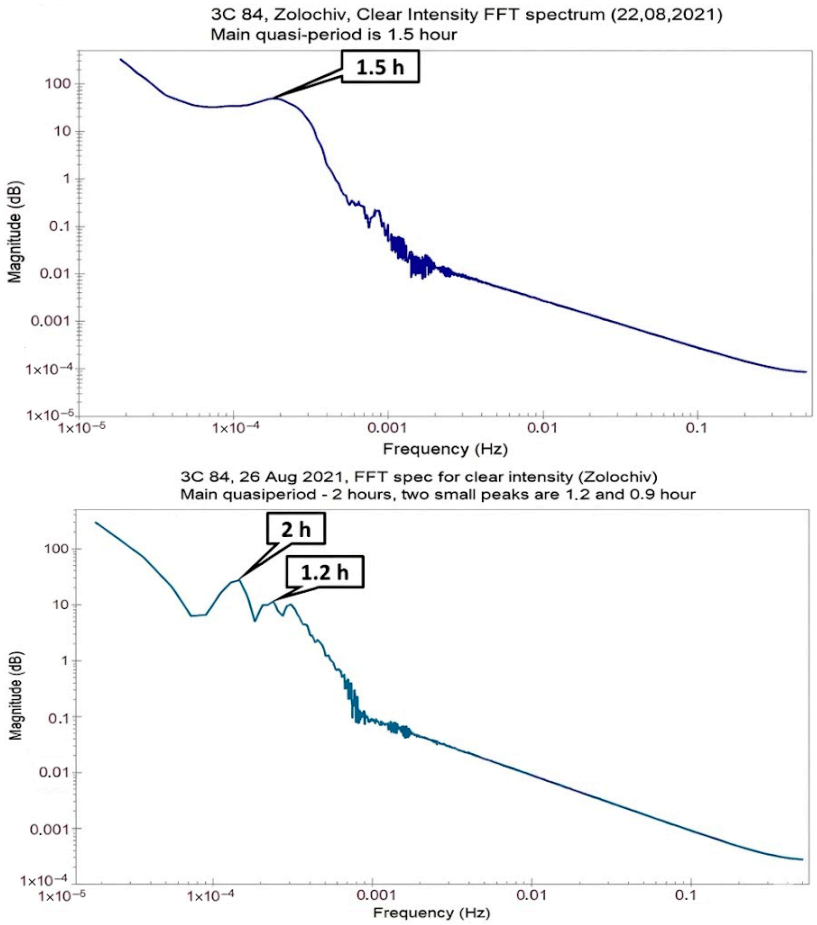

Figure 12. Fast Fourier Transform (FFT) spectra of brightness temperature variations in the radio source 3C 84 at a frequency of 6.5 GHz. (**Top panel**): Observations from 22 to 23 August 2021. (**Bottom panel**): Observations from 26 to 27 August 2021. The spectra highlight dominant fluctuation frequencies associated with intraday variability.

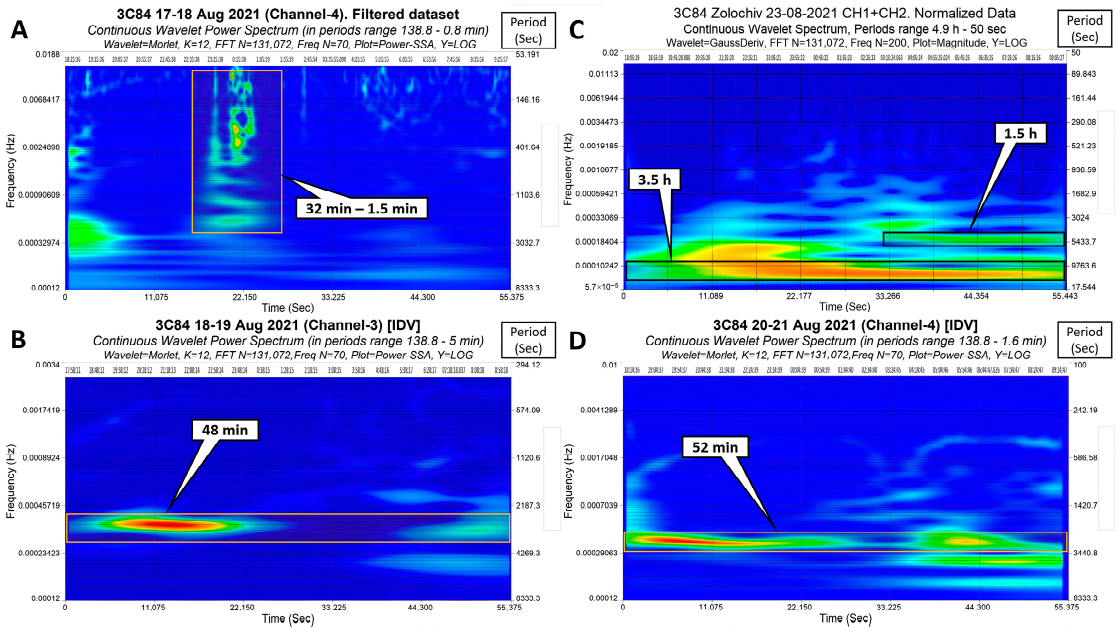

Figure 13. Examples of wavelet spectra from selected observation sessions of the radio source 3C 84. (**A**) Session from 17 to 18 August 2021: A ~2.5 h burst of variability is observed across periods ranging

from 1.5 to 32 min, with a transition from quasi-harmonic to noise-like structure. Notably, weak geomagnetic disturbances were present during this session. (**B**) Session from 18 to 19 August 2021: quasi-periodic variations with a period of approximately 48 min and total duration of ~5 h are evident. (**C**) Session from 23 to 24 August 2021: a more complex spectrum is observed, featuring a dominant quasi-period of ~3.5 h, along with a secondary feature in the latter half of the data near ~1.5 h. (**D**) Session from 20 to 21 August 2021: a well-defined quasi-period of ~52 min is present, with a longer persistence than in previous sessions. The color scale indicates correlation strength: from dark blue (no correlation) to red (strongest correlation).

Transient features of ~2 h duration in the radio flux time series—especially those with broad spectral content spanning from a few minutes to tens of minutes—are likely associated with ionospheric effects. In contrast, narrow-band features with clearly defined quasi-periods are more difficult to attribute solely to the ionosphere. Similar IDV patterns have been observed in other extragalactic sources and are commonly interpreted as interstellar scintillation (ISS), particularly at frequencies above 8 GHz [54,55].

At present, only a few radio sources are known to exhibit "intra-hour" variability, with typical timescales around or below one hour [56]. This type of variability is attributed to ISS caused by compact, high-density electron clouds in the local interstellar medium ($n_e \approx 10^2$ cm^{-3}), located at distances of 1–10 pc. The formation and stability mechanisms of such plasma structures remain poorly understood.

For 3C 84, IDV appears to occur sporadically—often for only a few days at a time—and most of the time the source exhibits noise-like variations (see Figure 14). However, observed quasi-periodic flux modulations in the 1–6 h range correspond well with expected AGW periods [57–59]. It is difficult to distinguish between ISS- and AGW-induced variability using a single-dish radio telescope, as both effects can operate on similar timescales. A possible solution is to conduct simultaneous, same-frequency observations using widely separated antennas.

We conducted test observations using the 32 m telescope of the Ventspils International Radio Astronomy Centre (VIRAC)[3] in Latvia [60,61]. The parameters of the RT-32 VIRAC radio telescope located in Latvia are presented in the paper [62]. Due to technical limitations, no reliable results were obtained in 2020–2021. However, one successful dual-station session was performed on 20 December 2020 using the RT-32 Zolochiv and VIRAC telescopes at 5 GHz. Cross-spectral FFT analysis revealed a strong coherence peak at a period of ~6 h. This result was described in detail in the paper [63], which also presents other results of the IDV study on the RT-32 Zolochiv and VIRAC radio telescopes. Nonetheless, further confirmation is required.

As a broader conclusion for studies of variable and transient cosmic radio sources, we emphasize the need to equip centimetre-wavelength radio telescopes with dedicated systems for monitoring signal propagation conditions in the lower atmosphere. These include: (i) ground-based meteorological sensors to monitor ambient temperature, pressure, humidity, dew point, and horn status; (ii) radiometric systems to assess total atmospheric attenuation (e.g., K-band radiometers or 3 mm atmospheric brightness temperature monitors); and (iii) systems for measuring total electron content and visualizing TIDs using GNSS station data [64,65]. These tools are essential for understanding the environmental contributions to variability in radio astronomical data.

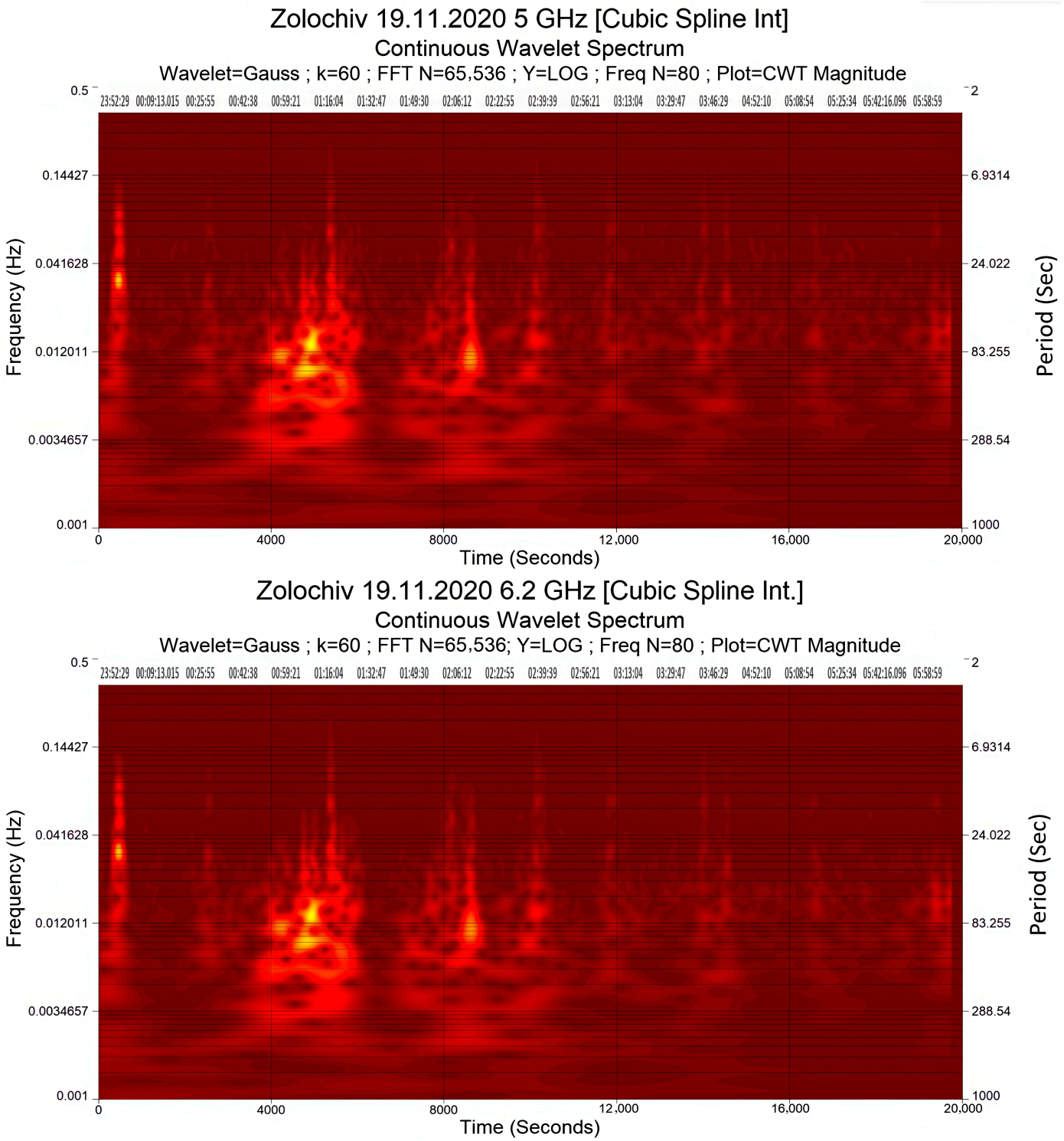

Figure 14. Wavelet power spectra of the radio source 3C 84 observed on 19 November 2020 with the RT-32 Zolochiv radio telescope at frequencies of 5 GHz (**top panel**) and 6.2 GHz (**bottom panel**). Dark red indicates the background with no correlation, while increasing correlation is shown by lighter red shades, reaching yellow at maximum correlation. The spectra indicate the absence of significant intraday variability (IDV), displaying only noise-like fluctuations in the source flux at both frequencies.

4. Discussion

The application of a novel observational technique in this study has provided new insights into the nature of IDV observed in the radio galaxy 3C 84. Specifically, the results

suggest that a substantial portion of the recorded short-term intensity fluctuations can be attributed to variations in radio wave propagation conditions within the Earth's ionosphere and lower atmosphere. In summertime conditions, the passage of the solar terminator across the observation site can result in dew formation on the radio-transparent coating of the beam waveguide (BWG) radio telescope system. Over intervals of one to two hours, this effect may lead to a noticeable attenuation of the radio signal from the observed source. Consequently, the observed intensity fluctuation spectrum becomes enriched with false periodicities that might otherwise be mistakenly interpreted as intrinsic variability of the source.

The use of the quasi-simultaneous measurement method enabled us to derive an upper estimate of the influence of AGWs and TIDs on ionospheric plasma parameters. While AGW/TID activity does intensify near the terminator, our results indicate that its contribution to IDV is generally smaller than that caused by dew accumulation on telescope components.

It is important to note that the current observation strategy—based solely on azimuthal scanning—limits our ability to fully characterize refractive effects arising from electron density irregularities along the line of sight. Incorporating elevation scanning would introduce a confounding modulation in the system temperature, due to varying levels of thermal noise from the Earth's surface as the elevation angle changes.

Overall, the IDV phenomenon in AGNs remains a challenging and unresolved problem in astrophysics. Models assuming an "intrinsic" origin—such as dynamic processes within the AGN core, accretion disc, or relativistic jets—lead to complex scenarios that currently lack definitive observational confirmation. While it is widely accepted that sub-hour variability is often caused by propagation effects (e.g., ionospheric irregularities or solar wind structures), a small subset of AGNs exhibit ultra-fast "intra-hour" variability that cannot be easily explained by Earth-based effects alone. The prevailing explanation for these cases involves ISS arising from turbulent plasma clouds in the local interstellar medium. Long-term monitoring of such sources has revealed an annual modulation in variability timescales, interpreted as the Earth's orbital motion relative to the scattering screen [66]. However, this effect is not universally observed, and the spatial distribution of these scattering screens remains poorly constrained.

In the present study, we observed low-amplitude intraday variations in the radio flux of 3C 84. While the physical origin of these fluctuations remains uncertain, the evidence clearly indicates that natural phenomena near the Earth—such as the diurnal passage of the solar terminator, dew formation, cloud presence, and ionospheric restructuring—make a significant contribution to observed variability in the C-band. This underscores a broader principle: any highly sensitive radio telescope operating at centimetre wavelengths also serves as a sensitive detector of environmental changes, including those in the lower atmosphere, ionosphere, and even interplanetary and interstellar media.

In this work, we did not account for the contribution of interplanetary scintillation, since the time resolution and integration parameters of the receiver effectively smoothed out these fluctuations. Likewise, we cannot yet reliably disentangle interstellar scintillation from variability caused by near-Earth atmospheric and ionospheric effects, given the overlap in their characteristic timescales. The possibility of intrinsic, short-timescale modulation of the source's emission remains an open question. Consequently, future studies of AGN IDV will require more sophisticated observational strategies—ideally involving multi-frequency, multi-station, and multi-parameter monitoring approaches to fully separate intrinsic, ionospheric, and interstellar contributions.

5. Conclusions

An improved observational technique for studying radio sources in the C band using a single-dish radio telescope has been developed and successfully implemented. The method is based on the joint analysis of two components of antenna temperature: the brightness temperature of the radio source and the system noise temperature of the telescope. These components are separated by introducing low-amplitude ($\leq 0.5^\circ$) azimuthal scanning, which modulates the telescope beam pattern without significantly altering the elevation angle or thermal background.

During the observational session of 22–23 August 2021, a pulsed radio burst was detected from the direction of the radio galaxy Perseus A (3C 84). The burst exhibited properties consistent with those of FRBs, though confirmation will require further observations.

Observations at 6.5 GHz revealed the presence of low-intensity IDV in the brightness temperature of 3C 84. This variability spans a spectral range from approximately 0.5×10^{-4} Hz to 1×10^{-3} Hz, corresponding to temporal scales between 0.27 and 5.56 h. Continuous wavelet transform and bandpass filtering techniques confirmed the occurrence of numerous IDV events at both 5 and 6.5 GHz. The timescales of variability differed significantly between sessions, most commonly falling within the 3–6 h range. Notably, quasi-harmonic variations with periods of approximately 1 h and 40–50 min were also detected. In addition to these active phases, the source occasionally exhibited calm periods with no significant flux density modulation.

The likely drivers of the observed variability include the passage of the solar terminator across the observation site—resulting in dew formation on the telescope structure—as well as ionospheric restructuring and, to a lesser extent, AGW and TID effects. The combination of these propagation phenomena may mimic intrinsic variability in the radio source.

However, single-dish observations do not allow for reliable discrimination between ionospheric and interstellar scintillation effects. To resolve this ambiguity, simultaneous multi-frequency observations using widely separated radio telescopes are necessary.

An upper bound on the contribution of AGW/TID-induced fluctuations has been established. Under geomagnetically quiet conditions, and in the absence of strong seismic or volcanic activity, the standard deviation of brightness temperature fluctuations attributable to AGW/TID does not exceed 0.076 K.

These findings emphasize the need to account for local meteorological and geophysical conditions when interpreting high-sensitivity radio observations. The development of integrated monitoring systems—including weather sensors, radiometers, and ionospheric diagnostics (e.g., GNSS-based TEC monitoring)—is essential for distinguishing between astrophysical and propagation-induced variability in radio astronomy.

Author Contributions: Conceptualization, V.B., O.U., A.S., V.Z., M.R., V.O., V.V. (Volodymyr Vlasenko), A.P., O.K., E.A., M.P., V.V. (Viktor Voityuk), V.C., D.B., D.Z. and M.K.; methodology, V.B., O.U., A.S., V.Z. and M.R.; software, O.U., A.S. and V.Z.; validation, O.U., A.S., V.Z., M.R. and V.O.; formal analysis, V.B., O.U., A.S., V.Z., M.R., V.C., D.B. and D.Z.; investigation, V.B., O.U., A.S., V.Z., M.R., V.O., V.V. (Volodymyr Vlasenko), A.P., O.K., E.A., M.P., V.V. (Viktor Voityuk), V.C., D.B., D.Z., I.S. and M.K.; resources, O.U., V.Z., V.O., V.V. (Volodymyr Vlasenko), A.P., O.K., E.A., M.P., V.V. (Viktor Voityuk), V.C. and D.B.; data curation, O.U., A.S., V.Z., M.R., V.O., V.V. (Volodymyr Vlasenko), A.P., O.K., E.A., V.V. (Viktor Voityuk) and D.B.; writing—original draft preparation, V.B., O.U., A.S., V.Z., M.R., O.K. and M.P.; writing—review and editing, V.B., O.U., A.S., V.Z., M.R., V.O., V.V. (Volodymyr Vlasenko), A.P., O.K., E.A., M.P., V.V. (Viktor Voityuk), V.C., D.B., D.Z., I.S. and M.K.; visualization, V.B., O.U. and A.S.; supervision, V.B., O.U., A.S., V.Z., O.K., M.P. and V.C.; project administration, V.B. and O.U.; funding acquisition, V.B., O.U., A.S., V.Z. and M.R. All authors have read and agreed to the published version of the manuscript.

Funding: V.B. received support from the Latvian Council of Science Fundamental and Applied Research project "Multi-Wavelength Study of Quasi-Periodic Pulsations in Solar and Stellar Flares (STEF) project No. lzp-2022/1-0017. A.S. received support from the research project "Research on Space Weather During Solar Cycle 25 Observed Along the 'Struve Geodetic Arc'", project No. 1.1.1.9/LZP/1/24/048 under the overarching project No. 1.1.1.9/1/24/I/001, co-financed by the European Regional Development Fund. The project is implemented within the European Union Cohesion Policy Programme 2021–2027, under specific support objective 1.1.1 "Strengthening Research and Innovation Capacity and the Introduction of Advanced Technologies in the Joint R&I System," activity 1.1.1.9 "Postdoctoral Research".

Data Availability Statement: The original contributions presented in this study are included in the article. Further inquiries can be directed to the corresponding authors.

Acknowledgments: E. Alekseev gratefully acknowledges financial support from the Centre National de la Recherche Scientifique (CNRS, France) and the Université de Lille (France). During the preparation of this manuscript, the authors used ChatGPT, based on the GPT-4.5 architecture, to assist with English grammar correction and stylistic improvements. All outputs were reviewed and edited by the authors, who take full responsibility for the final content of this publication.

Conflicts of Interest: The authors declare no conflicts of interest.

Abbreviations

The following abbreviations are used in this manuscript:

AGNs	Active Galactic Nuclei
AGW	Acoustic–Gravity Waves
ALMA	Atacama Large Millimetre/submillimetre Array
BWG	Beam Wave Guide
CWT	Continuous Wavelet Transform
DM	Dispersion Measure
FFT	Fast Fourier Transform
FRB	Fast Radio Burst
GNSS	Global Navigation Satellite System
IDV	Intraday Variability
ISS	Interstellar Scintillation
LCP	Left-hand Circular Polarization
MASIV	Micro-Arcsecond Scintillation-Induced Variability Survey
PSD	Power Spectral Density
RCP	Right-hand Circular Polarization
RT-32	32 m Radio Telescope
SMBH	Supermassive Black Hole
Sy1	Seyfert Type 1 Galaxy
Sy2	Seyfert Type 2 Galaxy
TEC	Total Electron Content
TID	Travelling Ionospheric Disturbance
VIRAC	Ventspils International Radio Astronomy Centre

Notes

1 Latvian Council of Science, Fundamental and Applied Research Project "Joint Latvian–Ukrainian Study of the Peculiar Radio Galaxy Perseus A in Radio and Optical Bands" (PERSEUS https://en.venta.lv/zinatne/projekti/joint-latvian-ukrainian-study-of-peculiar-radio-galaxy--perseus-a--in-radio-and-optical-bands, accessed on 17 December 2025)". No.: lzp-2020/2-0121. Duration: 1 December 2020–31 December 2021. Budget 100 kEuro.

2 VolcanoDiscovery (https://www.volcanodiscovery.com/, accessed on 17 December 2025)—Informational website providing updates on volcanic activity and related natural phenomena, including earthquake alerts.

3 Engineering Research Institute Ventspils International Radio Astronomy Centre (ERI VIRAC, https://en.venta.lv/virac accessed on 22 December 2025) of Ventspils University of Applied Sciences.

References

1. Netzer, H. Revisiting the Unified Model of Active Galactic Nuclei. *Annu. Rev. Astron. Astrophys.* **2015**, *53*, 365–408. [CrossRef]
2. Padovani, P.; Alexander, D.M.; Assef, R.J.; De Marco, B.; Giommi, P.; Hickox, R.C.; Salvato, M. Active galactic nuclei: What's in a name? *Astron. Astrophys. Rev.* **2017**, *25*, 2. [CrossRef]
3. Lal, D.V.; Shastri, P.; Gabuzda, D.C. Seyfert galaxies: Nuclear radio structure and unification. *Astrophys. J.* **2011**, *731*, 68. Available online: https://iopscience.iop.org/article/10.1088/0004-637X/731/1/68 (accessed on 17 December 2025). [CrossRef]
4. Britzen, S.; Fendt, C.; Zajacek, M.; Jaron, F.; Pashchenko, I.; Aller, M.F.; Aller, H.D. 3C 84: Observational Evidence for Precession and a Possible Relation to TeV Emission. *Galaxies* **2019**, *7*, 72. [CrossRef]
5. Gorshkov, A.G.; Ipatov, A.V.; Ipatova, I.A.; Konnikova, V.K.; Mardyshkin, V.V.; Mingaliev, M.G.; Kharinov, M.A. Long-Term and Rapid Radio Variability of the Blazar 3C 454.3 in 2010–2017. *Astron. Rep.* **2018**, *62*, 183–199. [CrossRef]
6. Epstein, E.E.; Landau, R.; Rather, J.D.G. Extragalactic radio sources—Rapid variability at 90 GHz. *Astron. J.* **1980**, *85*, 1427–1433. Available online: https://ui.adsabs.harvard.edu/abs/1980AJ.....85.1427E/abstract (accessed on 17 December 2025). [CrossRef]
7. Vieyro, F.L.; Romero, G.E.; Bosch-Ramon, V.; Marcote, B.; del Valle, M.V. A model for the repeating FRB 121102 in the AGN scenario. *Astron. Astrophys.* **2017**, *602*, A64. [CrossRef]
8. Shannon, R.M.; Ravi, V. Radio-Interferometric Monitoring of FRB 131104: A Coincident AGN Flare, but No Evidence for a Cosmic Fireball. *Astrophys. J. Lett.* **2017**, *837*, L22. [CrossRef]
9. Chatterjee, S.; Law, C.J.; Wharton, R.S.; Burke-Spolaor, S.; Hessels, J.W.T.; Bower, G.C.; van Langevelde, H.J. A direct localization of a fast radio burst and its host. *Nature* **2017**, *541*, 58–61. [CrossRef]
10. Nimmo, K.; Hessels, J.W.T.; Snelders, M.P.; Karuppusamy, R.; Hewitt, D.M.; Kirsten, F.; Yuan, J. A burst storm from the repeating FRB 20200120E in an M81 globular cluster. *Mon. Not. R. Astron. Soc.* **2023**, *520*, 2281–2305. [CrossRef]
11. Hewitt, D.M.; Bhardwaj, M.; Gordon, A.C.; Kirichenko, A.; Nimmo, K.; Bhandari, S.; Yuan, J.P. A Repeating Fast Radio Burst Source in a Low-luminosity Dwarf Galaxy. *Astrophys. J.* **2024**, *977*, L4. [CrossRef]
12. Wolszczan, A.; Cordes, J.; Stinebring, D. A Single Pulse Study of the Millisecond Pulsar 1937+214 (Poster). In *Birth and Evolution of Neutron Stars: Issues Raised by Millisecond Pulsars*; National Radio Astronomy Observatory (NRAO): Green Bank, WV, USA, 1984; p. 63. Available online: https://articles.adsabs.harvard.edu/pdf/1984bens.work...63W (accessed on 17 December 2025).
13. Popov, M.V.; Kuz'min, A.D.; Ul'yanov, O.M.; Deshpande, A.A.; Ershov, A.A.; Zakharenko, V.V.; Kondrat'ev, V.I.; Kostyuk, S.V.; Losovski, B.Y.; Soglasnov, V.A. Instantaneous Radio Spectra of Giant Pulses from the Crab Pulsar from Decimeter to Decameter Wavelengths. *Astron. Rep.* **2006**, *50*, 562–568. Available online: https://link.springer.com/article/10.1134/S1063772906070067 (accessed on 17 December 2025).
14. Ulyanov, O.M.; Skoryk, A.O.; Shevtsova, A.I.; Plakhov, M.S.; Ulyanova, O.O. Detection of the fine structure of the pulsar J0953+0755 radio emission in the decametre wave range. *Mon. Not. R. Astron. Soc.* **2015**, *455*, 150–157. [CrossRef]
15. Bilous, A.V.; Grießmeier, J.M.; Pennucci, T.; Wu, Z.; Bondonneau, L.; Kondratiev, V.; van Leeuwen, J.; Maan, Y.; Connor, L.; Oostrum, L.C.; et al. Dual-frequency single-pulse study of PSR B0950+08. *Astron. Astrophys.* **2022**, *658*, A143. [CrossRef]
16. Bhardwaj, M.; Gaensler, B.M.; Kaspi, V.M.; Landecker, T.L.; Mckinven, R.; Michilli, D.; Pleunis, Z.; Tendulkar, S.P.; Andersen, B.C.; Boyle, P.J.; et al. A Nearby Repeating Fast Radio Burst in the Direction of M81. *Astrophys. J. Lett.* **2021**, *910*, L18. [CrossRef]
17. Hewitt, D.M.; Bhandari, S.; Marcote, B.; Hessels, J.W.; Nimmo, K.; Kirsten, F.; Yuan, J.P. Milliarcsecond localization of the hyperactive repeating FRB 20220912A. *Mon. Not. R. Astron. Soc.* **2024**, *529*, 1814–1826. [CrossRef]
18. Bannikova, E.Y.; Sergeyev, A.V.; Akerman, N.A.; Berczik, P.P.; Ishchenko, M.V.; Capaccioli, M.; Akhmetov, V.S. Dynamical model of an obscuring clumpy torus in AGNs—I. Velocity and velocity dispersion maps for interpretation of ALMA observations. *Mon. Not. R. Astron. Soc.* **2021**, *503*, 1459–1472. [CrossRef]
19. Bannikova, E.Y.; Akerman, N.O.; Capaccioli, M.; Berczik, P.P.; Akhmetov, V.S.; Ishchenko, M.V. Apparent counter-rotation in the torus of NGC 1068: Influence of an asymmetric wind. *Mon. Not. R. Astron. Soc.* **2023**, *518*, 742–751. [CrossRef]
20. Sukharev, A.; Ryabov, M.; Bezrukovs, V.; Ul'yanov, O.; Udovichenko, S.; Keir, L.; Dubovskii, P.; Kudzej, I.; Konovalenko, A.; Zakharenko, V.; et al. Study of the Rapid Variability of the BL Lac Object MRK 421 in the Optical Range. *Astrophysics* **2022**, *65*, 1–18. [CrossRef]
21. Hines, C.O. Internal Atmospheric Gravity Waves at Ionospheric Heights. *Can. J. Phys.* **1960**, *38*, 1441–1481. [CrossRef]
22. Hines, C.O.; Reddy, C.A. On the Propagation of Atmospheric Gravity Waves through Regions of Wind Shear. *J. Geophys. Res.* **1967**, *72*, 1015–1034. [CrossRef]
23. Cheremnykh, O.K.; Selivanov, Y.A.; Zakharov, I.V. The influence of compressibility and nonisothermality of the atmosphere on the propagation of acousto-gravity waves. *Kosm. Nauka Tekhnol.* **2010**, *16*, 9–19. [CrossRef]
24. Jauncey, D.L.; Bignall, H.E.; Kedziora-Chudczer, L.; Koay, J.Y.; Lovell, J.E.J.; Macquart, J.-P.; Ojha, R.; Pursimo, T.; Reynolds, C.; Rickett, B. Interstellar Scintillation and Scattering of Micro-arc-second AGN. *Galaxies* **2016**, *4*, 62. [CrossRef]
25. Béniguel, Y.; Adam, J.-P.; Prieto-Cerdeira, R.; Arbesser-Rastburg, B. Ionospheric Scintillations at L & C Bands. In Proceedings of the 3rd European Conference on Antennas and Propagation (EuCAP 2009), Berlin, Germany, 23–27 March 2009; pp. 1–5. Available online: https://www.vde-verlag.de/proceedings-en/453152876.html (accessed on 17 December 2025).

26. Jakowski, N.; Mayer, C.; Wilken, V.; Hoque, M.M. Ionospheric Impact on GNSS Signals. *Física De La Tierra* **2008**, *20*, 11–25. Available online: https://revistas.ucm.es/index.php/FITE/article/view/FITE0808110011A/11458 (accessed on 17 December 2025).
27. Taur, R.R. Ionospheric scintillation at frequencies above 1 GHz. *COMSAT Tech. Rev.* **1974**, *4*, 461–476. Available online: https://ui.adsabs.harvard.edu/abs/1974COMTR...4..461T/abstract (accessed on 17 December 2025).
28. Davies, K.; Smith, E.K. Ionospheric effects on satellite land mobile systems. *IEEE Antennas Propag. Mag.* **2002**, *44*, 24–31. [CrossRef]
29. Sukharev, A.; Ryabov, M.; Bezrukovs, V.; Ulyanov, O.; Udovichenko, S.; Keir, L.; Dubovsky, P.; Kudzej, I.; Konovalenko, A.; Zakharenko, V.; et al. Results of studying the radio and optical variability properties of MRK 501 active galaxy. *Astron. Astrophys. Trans.* **2022**, *33*, 45–66. [CrossRef]
30. Kaladze, T.; Pokhotelov, O.A.; Shah, H.; Khan, M.I. Acoustic-Gravity Waves in the Earth's Ionosphere. *J. Atmos. Sol.-Terr. Phys.* **2008**, *70*, 1607–1616. [CrossRef]
31. Cheremnykh, O.K.; Fedorenko, A.K.; Kryuchkov, E.I.; Selivanov, Y.A. Evanescent acoustic-gravity modes in the isothermal atmosphere: Systematization and applications to the Earth and solar atmospheres. *Ann. Geophys.* **2019**, *37*, 405–415. [CrossRef]
32. NEC Corporation. MARK-4B. In *Operation and Maintenance Handbook for Antenna Subsystem*; Book 1, Part 1; Antenna Structure: Tokyo, Japan, 1986.
33. Woodburn, L.; Natusch, T.; Weston, S.; Thomasson, P.; Godwin, M.; Granet, C.; Gulyaev, S. Conversion of a New Zealand 30-metre telecommunications antenna into a radio telescope. *Publ. Astron. Soc. Aust.* **2015**, *32*, e017. [CrossRef]
34. Petrov, L.; Natusch, T.; Weston, S.; McCallum, J.; Ellingsen, S.; Gulyaev, S. First scientific VLBI observations using New Zealand 30-m radio telescope WARK30M. *Publ. Astron. Soc. Pac.* **2015**, *127*, 516–522. [CrossRef]
35. Yonekura, Y.; Saito, Y.; Sugiyama, K.; Soon, K.L.; Momose, M.; Yokosawa, M.; Ogawa, H.; Kimura, K.; Abe, Y.; Nishimura, A.; et al. The Hitachi and Takahagi 32-m radio telescopes: Upgrade of the antennas from satellite communication to radio astronomy. *Publ. Astron. Soc. Jpn.* **2016**, *68*, 74. [CrossRef]
36. Ulyanov, O.M.; Reznichenko, O.M.; Zakharenko, V.V.; Antyufeyev, A.V.; Korolev, A.M.; Patoka, O.M.; Prisiazhnii, V.I.; Poikhalo, A.V.; Voityuk, V.V.; Mamarev, V.N.; et al. Creating the RT-32 Radio Telescope on the Basic of MARK-4B Antenna System. 1. Modernization Project and First Results. *Radio Phys. Radio Astron.* **2019**, *24*, 87–116. [CrossRef]
37. Antyufeyev, A.V.; Korolev, A.M.; Patoka, O.M.; Shulga, V.M.; Ulyanov, O.M.; Reznichenko, O.M.; Zakharenko, V.V.; Prisiazhnii, V.I.; Poikhalo, A.V.; Voityuk, V.V.; et al. Creating the RT-32 Radio Telescope on the Basic of MARK-4B Antenna System. 2. Estimation of the Possibility for Making Spectral Observations of Radio Astronomical Objects. *Radio Phys. Radio Astron.* **2019**, *24*, 163–183. [CrossRef]
38. Ulyanov, O.M.; Zakharenko, V.V.; Alekseev, E.A.; Reznichenko, O.M.; Kulahin, I.O.; Budnikov, V.V.; Prysiazhnii, V.I.; Poikhalo, A.V.; Voitiuk, V.V.; Mamariev, V.M.; et al. The RT-32 Radio Telescope Construction Based on the MARK-4B Antenna System. 3. Local Oscillators and Self-Noise of the Receiving System. *Radio Phys. Radio Astron.* **2020**, *25*, 175–192. [CrossRef]
39. Williams, W.F.; Withington, J.R. A Common Aperture S- and X-Band Feed for the Deep Space Network. In Proceedings of the Antenna Applications Symposium; Monticello, IL, USA, 23–25 September 1981. Available online: https://ntrs.nasa.gov/citations/19830053868 (accessed on 17 December 2025).
40. Imbriale, W.A. *Large Antennas of the Deep Space Network*; Monograph 4, Deep–Space Communications and Navigation Series; Jet Propulsion Laboratory, California Institute of Technology: Pasadena, CA, USA, 2002. Available online: https://descanso.jpl.nasa.gov/monograph/series4/Descanso_Mono4_web.pdf (accessed on 17 December 2025).
41. Vlasenko, V.P.; Mamarev, V.M.; Ozhinskyi, V.V.; Ulyanov, O.M.; Zakharenko, V.V.; Palamar, M.I.; Chaikovskyi, A.V. Method of Constructing the Primary Error Matrix of the RT-32 Radio Telescope in an Automated Mode. *Chin. Space Sci. Technol.* **2021**, *27*, 66–75. [CrossRef]
42. Foschi, M.; Gomez, J.L.; Fuentes, A.; Cho, I.; Marscher, A.P.; Jorstad, S. Evolution, speed, and precession of the parsec-scale jet in the 3C 84 radio galaxy. *Astron. Astrophys.* **2025**, *696*, A17. [CrossRef]
43. Savolainen, T.; Giovannini, G.; Kovalev, Y.Y.; Perucho, M.; Anderson, J.M.; Bruni, G.; Zensus, J.A. RadioAstron discovery of a mini-cocoon around the restarted parsec-scale jet in 3C 84. *Astron. Astrophys.* **2023**, *676*, A114. [CrossRef]
44. Gorry, P.A. General least-squares smoothing and differentiation by the convolution (Savitzky–Golay) method. *Anal. Chem.* **1990**, *62*, 570–573. [CrossRef]
45. Andersen, B.C.; Bandura, K.; Bhardwaj, M.; Boyle, P.J.; Brar, C.; Zwaniga, A. Sub-second Periodicity in a Fast Radio Burst. *Nature* **2022**, *607*, 256–259. [CrossRef]
46. Zhang, B. A "Cosmic Comb" Model of Fast Radio Bursts. *Astrophys. J. Lett.* **2017**, *836*, L32. [CrossRef]
47. Kirsten, F.; Marcote, B.; Nimmo, K.; Hessels, J.W.T.; Bhardwaj, M.; Tendulkar, S.P.; Vlemmings, W. A repeating fast radio burst source in a globular cluster. *Nature* **2022**, *602*, 585–589. [CrossRef]
48. Nimmo, K.; Hewitt, D.M.; Hessels, J.W.T.; Kirsten, F.; Marcote, B.; Bach, U.; Blaauw, R.; Burgay, M.; Corongiu, A.; Feiler, R.; et al. Milliarcsecond Localization of the Repeating FRB 20201124A. *Astrophys. J. Lett.* **2022**, *927*, L3. [CrossRef]
49. Rishbeth, H. The ionospheric E-layer and F-layer dynamos—A tutorial review. *J. Atmos. Sol.-Terr. Phys.* **1997**, *59*, 1873–1880. [CrossRef]

50. Zhang, M.-L.; Liu, C.; Wan, W.; Liu, L.; Ning, B. A global model of the ionospheric F2 peak height based on EOF analysis. *Ann. Geophys.* **2009**, *27*, 3203–3212. [CrossRef]
51. Pleunis, Z.; Michilli, D.; Bassa, C.G.; Hessels, J.W.T.; Naidu, A.; Andersen, B.C.; Chawla, P.; Fonseca, E.; Gopinath, A.; Kaspi, V.M.; et al. LOFAR Detection of 110–188 MHz Emission and Frequency-dependent Activity from FRB 20180916B. *Astrophys. J. Lett.* **2021**, *911*, L3. [CrossRef]
52. Kumar, V.; Ghosh, S.; Parida, M.K.; Albert, S.K. Application of Continuous Wavelet Transform Based on Fast Fourier Transform for the Quality Analysis of Arc Welding Process. *Int. J. Syst. Assur. Eng. Manag.* **2023**, *15*, 917–930. [CrossRef]
53. Kirby, J. The Continuous Wavelet Transform. In *Spectral Methods for the Estimation of the Effective Elastic Thickness of the Lithosphere*; Springer: Cham, Switzerland, 2022; pp. 41–63. [CrossRef]
54. Bignall, H.E.; Jauncey, D.L.; Lovell, J.E.J.; Tzioumis, A.K.; Kedziora-Chudczer, L.; Macquart, J.-P.; Tingay, S.J.; Rayner, D.P.; Clay, R.W. Rapid Variability and Annual Cycles in the Characteristic Timescale of the Scintillating Source PKS 1257–326. *Astrophys. J.* **2003**, *585*, 653–665. [CrossRef]
55. Rickett, B.J.; Kedziora-Chudczer, L.; Jauncey, D.L. Interstellar Scintillation of the Polarized Flux Density in Quasar PKS 0405-385. *Astrophys. J.* **2002**, *581*, 103–126. [CrossRef]
56. de Bruyn, A.G.; Macquart, J.-P. The Intra-Hour Variable Quasar J1819+3845: 13-Year Evolution, Jet Polarization Structure, and Interstellar Scattering Screen Properties. *Astron. Astrophys.* **2015**, *574*, A125. [CrossRef]
57. Barabash, V.; Chernogor, L.; Panasenko, S.; Domnin, I. *Ionospheric Manifestations of Acoustic-Gravity Waves under Quiet and Disturbed Conditions*; EGU General Assembly: Vienna, Austria, 2014; p. 6162. Available online: https://meetingorganizer.copernicus.org/EGU2014/EGU2014-6162.pdf (accessed on 17 December 2025).
58. Ogunsua, B.O.; Qie, X.; Srivastava, A.; Abe, O.E.; Owolabi, C.; Jiang, R.; Yang, J. Ionospheric Perturbations Due to Large Thunderstorms and the Resulting Mechanical and Acoustic Signatures. *Remote Sens.* **2023**, *15*, 2572. [CrossRef]
59. Dominici, P.; Cander, L.R.; Zolesi, B. On the Origin of Medium-Period Ionospheric Waves and Their Possible Modelling: A Short Review. *Ann. Geophys.* **1997**, *41*, 1171–1178. Available online: https://www.researchgate.net/publication/288531168_On_the_origin_of_medium-period_ionospheric_waves_and_their_possible_modelling_A_short_review/fulltext/57a7afe508ae3f452939151f/On-the-origin-of-medium-period-ionospheric-waves-and-their-possible-modelling-A-short-review.pdf (accessed on 17 December 2025).
60. Bezrukovs, V. Receiving And Data Acquisition Systems Of RT-32 For VLBI Observations. *Latv. J. Phys. Tech. Sci.* **2012**, *49*, 30–42. [CrossRef]
61. Bezrukovs, V. Time and Frequency Synchronization on the Virac Radio Telescope RT-32. *Latv. J. Phys. Tech. Sci.* **2016**, *53*, 14–19. [CrossRef]
62. Skirmante, K.; Eglitis, I.; Jekabsons, N.; Bezrukovs, V.; Bleiders, M.; Nechaeva, M.; Jasmonts, G. Observations of astronomical objects using radio (Irbene RT-32 telescope) and optical (Baldone Schmidt) methods. *Astron. Astrophys. Trans.* **2019**, *32*, 13–22. [CrossRef]
63. Sukharev, A.; Ryabov, M.; Bezrukovs, V.; Orbidans, A. Investigation of intra-day variability of the radio galaxy 3C 84 (Perseus A) flux density in centimeter range on the RT-32 VIRAC (Latvia) and RT-32 NSFCTC (Ukraine) radio telescopes. *Astron. Astrophys. Trans.* **2022**, *33*, 149–174. [CrossRef]
64. Paznukhov, V.V.; Sopin, A.A.; Galushko, V.G.; Kashcheyev, A.S.; Koloskov, A.V.; Yampolski, Y.M.; Zalizovski, A.V. Occurrence and Characteristics of Traveling Ionospheric Disturbances in the Antarctic Peninsula Region. *J. Geophys. Res. Space Phys.* **2022**, *127*, e2022JA030895. [CrossRef]
65. Nykiel, G.; Zanimonskiy, Y.M.; Yampolski, Y.M.; Figurski, M. Efficient Usage of Dense GNSS Networks in Central Europe for the Visualization and Investigation of Ionospheric TEC Variations. *Sensors* **2017**, *17*, 2298. [CrossRef]
66. Bignall, H.E.; Jauncey, D.L.; Lovell, J.E.J.; Tzioumis, A.K.; Macquart, J.-P.; Kedziora-Chudczer, L. Observations of Intrahour Variable Quasars: Scattering in Our Galactic Neighbourhood. *Astron. Astrophys. Trans.* **2007**, *26*, 567–573. [CrossRef]